



# Discontinuous Galerkin methods for the numerical solution of the nonlinear Maxwell equations in 1d

Loula Fezoui, Stéphane Lanteri

## ► To cite this version:

Loula Fezoui, Stéphane Lanteri. Discontinuous Galerkin methods for the numerical solution of the nonlinear Maxwell equations in 1d. [Research Report] RR-8678, Inria. 2015. hal-01114155v2

**HAL Id: hal-01114155**

**<https://inria.hal.science/hal-01114155v2>**

Submitted on 11 Feb 2015

**HAL** is a multi-disciplinary open access archive for the deposit and dissemination of scientific research documents, whether they are published or not. The documents may come from teaching and research institutions in France or abroad, or from public or private research centers.

L'archive ouverte pluridisciplinaire **HAL**, est destinée au dépôt et à la diffusion de documents scientifiques de niveau recherche, publiés ou non, émanant des établissements d'enseignement et de recherche français ou étrangers, des laboratoires publics ou privés.



# Discontinuous Galerkin methods for the numerical solution of the nonlinear Maxwell equations in 1d

Loula Fezoui and Stéphane Lanteri

**RESEARCH  
REPORT**

**N° 8678**

January 2015

Project-Team Nachos





# Discontinuous Galerkin methods for the numerical solution of the nonlinear Maxwell equations in 1d

Loula Fezoui and Stéphane Lanteri\*

Project-Team Nachos

Research Report n° 8678 — January 2015 — 38 pages

**Abstract:** The system of Maxwell equations describes the evolution of the interaction of an electromagnetic field with a propagation medium. The different properties of the medium, such as isotropy, homogeneity, linearity, among others, are introduced through *constitutive laws* linking fields and inductions. In the present study, we focus on nonlinear effects and address nonlinear Kerr materials specifically. In this model, any dielectric may become nonlinear provided the electric field in the material is strong enough. This is even the case in vacuum but then the minimal amount of energy necessary to observe nonlinear effects is similar to the total energy produced by the sun in one second. We nonetheless use the vacuum as one of the two dielectrics in our numerical simulations. The other one is the air wherein the minimal electric field magnitude for observing nonlinear effects is  $10^6$  V/m, which can be achieved by lasers in production today. We will see that in some situations, such as when an oscillating electric dipole radiates in open space, frequency may also impact and even increase nonlinear effects. The work presented here is restricted to one dimensional space in order to compare numerical results to analytic solutions when possible, but all physical details and numerical techniques extend to higher dimensions without much difficulty.

**Key-words:** Maxwell's equations, time-domain, discontinuous Galerkin, nonlinear medium, Kerr model.

---

\* Inria, 2004 Route des Lucioles, BP 93 06902 Sophia Antipolis Cedex, France

# Résolution numérique des équations de Maxwell 1d par des méthodes Galerkin discontinues

**Résumé :** Le système des équations de Maxwell décrit l'évolution d'un champ électromagnétique en interaction avec un milieu de propagation. Les différentes propriétés de ce milieu, telles que son caractère isotrope ou anisotrope, homogène ou hétérogène, linéaire ou non-linéaire, sont définies par des lois constitutives qui lient champs et inductions. Dans cette étude, on s'intéresse aux effets non-linéaires et on considère plus particulièrement le cas de milieux non-linéaires de type Kerr. Dans le cas de ce modèle, n'importe quel diélectrique peut se comporter comme un matériau non-linéaire dès lors que l'amplitude du champ électrique se propageant dans le milieu est suffisamment forte. C'est par exemple le cas du vide mais l'énergie minimale pour observer des effets non-linéaires doit être similaire à l'énergie totale produite par le soleil en une seconde. Nous considérons néanmoins le vide comme un milieu candidat pour notre étude, au même titre que l'air. Pour ce dernier, l'amplitude minimale du champ électrique pour observer des effets non-linéaires est  $10^6$  V/m, un niveau qui peut être atteint par les lasers exploités de nos jours. Nous verrons que dans certaines situations, comme par exemple dans le cas d'un dipôle électrique oscillant en espace libre, la fréquence d'oscillation peut aussi impacter et même accroître les effets non-linéaires. Le travail présenté ici se limite au cas à une dimension d'espace pour pouvoir comparer les solutions numériques avec des solutions analytiques lorsque cela est possible, cependant tous les détails physiques et techniques numériques s'étendent aisément aux dimensions supérieures.

**Mots-clés :** équations de Maxwell, domaine temporel, Galerkin discontinu, milieu non-linéaire, modèle de Kerr.

## Contents

<b>1 Introduction</b>	<b>4</b>
<b>2 Mathematical model</b>	<b>4</b>
2.1 Derivation of the matrix $\mathcal{J}$	7
2.2 1d system	8
<b>3 Discontinuous Galerkin (DG) method</b>	<b>9</b>
3.1 Reference element	10
3.2 Limited polynomials	11
3.3 Finite volume method (FVM)	11
<b>4 Runge-Kutta scheme</b>	<b>12</b>
<b>5 Approximation of the E field</b>	<b>13</b>
5.1 Newton method	14
5.2 Padé Approximants	14
5.3 Euler method	14
<b>6 Electromagnetic energy</b>	<b>15</b>
<b>7 Numerical experiments</b>	<b>15</b>
7.1 Square-shaped pulse	16
7.2 Gaussian pulse	21
7.3 Wave packet	25
7.4 Electric dipole radiation	27
<b>8 Conclusion</b>	<b>31</b>
<b>Annexes</b>	<b>32</b>
<b>A Spectral analysis</b>	<b>32</b>
A.1 Eigenvalues and eigenvectors	32
A.2 Riemann invariants	32
<b>B Rescaling of the equations</b>	<b>34</b>
<b>C An implicit analytical solution [PNTB09]</b>	<b>36</b>
C.1 Formulation of the analytical solution	36
C.2 Estimation of $T_{\max}$	37

## 1 Introduction

The system of Maxwell equations describes the evolution of the interaction of an electromagnetic field with a propagation medium. The different properties of the medium, such as isotropy, homogeneity, linearity, among others, are introduced through *constitutive laws* linking fields and inductions. In the present study, we focus on nonlinear effects and address nonlinear Kerr materials specifically. In this model, any dielectric may become nonlinear provided the electric field in the material is strong enough. This is even the case in vacuum but then the minimal amount of energy necessary to observe nonlinear effects is similar to the total energy produced by the sun in one second. We will nonetheless use the vacuum as one of the two dielectrics in our numerical simulations. The other one is the air wherein the minimal electric field magnitude for observing nonlinear effects is  $10^6$  V/m, which can be achieved by lasers in production today. We will see that in some situations, such as when an oscillating electric dipole radiates in open space, frequency may also impact and even increase nonlinear effects. The work presented here is restricted to one dimensional space in order to compare numerical results to analytic solutions when possible, but all physical details and numerical techniques extend to higher dimensions without much difficulty.

For the numerical treatment of the Maxwell-Kerr model, the FDTD (Finite Difference Time-Domain) method [TH05] is often considered as the method of choice to simulate nonlinear effects such as the self-focusing of an ultrashort pulsed beam. We refer to [JT97] and [ZJ93] among other similar works. There exist only a few tentatives to investigate alternative numerical methods. In [FWR07], a full wave 3d vector finite element (FETD - Finite Element Time-Domain) method is presented that can be used to model nonlinear photonics effects in complicated geometries. A finite volume (FVTD - Finite Volume Time-Domain) method is introduced in [de 00]. This work seems to be the first tentative to import and adapt numerical schemes extensively studied for compressible fluid flow problems. More recently, a discontinuous Galerkin (DGTD - Discontinuous Galerkin Time-Domain) method is presented in [Bla13] for a certain 2d form of the full Maxwell-Kerr equations, but numerical experiments are limited to 1d problems. During the last 10 years, the DGTD method has been increasingly adopted for the solution of the time-domain Maxwell equations in the case of linear propagation media [HW02]-[FLLP05], and in particular for nanophotonics applications [BKN11]. We focus here on this latter family of methods and present the results of a preliminary numerical investigation in 1d.

## 2 Mathematical model

The system of time-domain Maxwell equations writes as

$$\begin{cases} \frac{\partial \mathbf{D}}{\partial t} &= \nabla \times \mathbf{H}, \\ \frac{\partial \mathbf{B}}{\partial t} &= -\nabla \times \mathbf{E}, \\ \nabla \cdot \mathbf{D} &= \rho, \\ \nabla \cdot \mathbf{B} &= \mathbf{J}, \end{cases} \quad (1)$$

where  $\mathbf{D}$  is the electric induction ( $\text{C/m}^2$ ),  $\mathbf{E}$  is the electric field ( $\text{V/m}$ ),  $\mathbf{B}$  the magnetic induction ( $\text{Vs/m}^2$  or  $\text{T}$ ),  $\mathbf{H}$  the magnetic field ( $\text{A/m}$ ),  $\mathbf{J}$  the current density ( $\text{A/m}^2$ ) and  $\rho$  the charge density ( $\text{C/m}^3$ ), all units in parentheses assuming the S.I. unit system. The inductions are linked to the fields through *constitutive laws* or *material laws* that account for the interaction of the electromagnetic field with the considered medium, and that are generally written as

$$\boxed{\mathbf{D} = \mathbf{D}(\mathbf{E}, \mathbf{H}), \quad \mathbf{B} = \mathbf{B}(\mathbf{E}, \mathbf{H})} \quad (2)$$

In practice, multipolar developments are used to formulate the inductions in terms of fields and moments (see [Jac99, p. 14]) but we only consider here dipolar moments and we write

$$\mathbf{D} = \varepsilon_0 \mathbf{E} + \mathbf{P}, \quad (3a)$$

$$\mathbf{B} = \mu \mathbf{H} - \mathbf{M}, \quad (3b)$$

where  $\mathbf{P}$  and  $\mathbf{M}$  denote the electric and magnetic dipolar moment densities respectively,  $\varepsilon_0$  is the electric permittivity of vacuum ( $\text{F/m}$  with  $\text{F}=\text{C/V}$ ) and  $\mu_0$  is the magnetic permeability of vacuum ( $\text{H/m}$  with  $\text{H}=\text{Vs/A}$ );  $\mathbf{P}$  and  $\mathbf{M}$  have the dimensions of  $\mathbf{D}$  and  $\mathbf{B}$  respectively.

Assuming that the magnitude of the exterior field  $\mathbf{E}$  is *small* compared to that of the characteristic field of the system (e.g. the field associated to atomic bonding), we can develop  $\mathbf{P}$  as a series of powers of  $\mathbf{E}$

$$\mathbf{P} = \varepsilon_0 \left( \chi^{(1)} \mathbf{E} + \chi^{(2)} \mathbf{E}^2 + \dots \chi^{(n)} \mathbf{E}^n + \dots \right), \quad (4)$$

where  $\chi^{(n)} = \chi^{(n)}(\mathbf{r}, \omega)$  denotes the electric susceptibility of order  $n$  which is a tensor of order  $(n+1)$ . This tensor can possibly depend on the spatial coordinate vector  $\mathbf{r}$  (i.e. in the case of an heterogeneous medium) and/or on the frequency  $\omega$  (i.e. in the case of a dispersive medium). In Eq. (4), the powers of the vectorial field  $\mathbf{E}$  must be understood as tensorial products

$$P_i^n = \varepsilon_0 \left[ \chi^{(n)} \mathbf{E}^n \right]_i = \sum_{j_1, j_2, \dots, j_{n+1}} \chi_{i, j_1, j_2, \dots, j_{n+1}}^{(n)} E_{j_1} E_{j_2} \dots E_{j_{n+1}}, \quad (5)$$

where  $U_i$  denotes the  $i^{\text{ème}}$  component of the vector  $\mathbf{U}$ . We now make the following hypotheses concerning the underlying propagation medium.

### Hypothesis 1.

*The medium is non-magnetic (i.e.  $\mu \approx \mu_0$ ).*

We can thus set  $\mu = \mu_0$  but we will keep the notation  $\mu$  for clarity.

### Hypothesis 2.

*The medium is isotropic.*

Then  $\chi^{(n)}(\mathbf{r}, \omega)$  is the product of a scalar function by the identity tensor of order  $n$  and we can deduce (thanks to symmetry arguments) that the moments of even order  $\chi^{(2)}, \chi^{(4)}, \dots$  are all zero (see [Bet09]).

### Hypothesis 3.

*The medium is homogeneous and non-dispersive.*



Then  $\chi^{(n)}$  is the product of a constant by the identity tensor of order  $n$ .

Under the hypotheses 2 and 3 and using the development (4) up to order 3, the polarization vector  $\mathbf{P}$  writes

$$\mathbf{P} = \varepsilon_0 \left( \chi_1 \mathbf{I}_d^{(2)} \mathbf{E} + \chi_3 \mathbf{I}_d^{(4)} \mathbf{E}^3 \right), \quad (6)$$

where  $\mathbf{I}_d^{(k)}$  is the identity tensor of order  $k$ , while  $\chi_1$  and  $\chi_3$  are constants. For  $k = 2$  we obtain the identity matrix (of  $\mathbb{R}^3$ ) and for  $k = 4$  we have

$$\mathbf{I}_d^{(4)}(i, j, k, l) = \delta_{ij} \delta_{kl}, \quad i, j, k, l = 1 \dots 3, \quad (7)$$

where  $\delta_{ij}$  is the Kronecker symbol. We recall that a tensor of order  $k$  in  $\mathbb{R}^n$  has  $n^k$  entries. Using Eq. (6) and (7) we find the expression of the polarization  $\mathbf{P}$  adopted for modeling the Kerr effect

$$\boxed{\mathbf{P} = \varepsilon_0 \chi_1 \mathbf{E} + \varepsilon_0 \chi_3 \|\mathbf{E}\|^2 \mathbf{E} = \mathbf{P}_L + \mathbf{P}_{NL}} \quad (8)$$

**Remark 1.**

Note that in expression (8) the first order susceptibility,  $\chi_1$ , is a quantity without dimension, while the third order susceptibility,  $\chi_3$ , has dimension  $(m/V)^2$ . More generally, the susceptibility of order  $n$  is measured in  $(m/V)^n$  in the S.I. unit system.

Applying hypotheses 1-2-3 and using Eq. (8) for  $\mathbf{P}$ , the constitutive laws become

$$\mathbf{D} = \varepsilon_0 (1 + \chi_1 + \chi_3 \|\mathbf{E}\|^2) \mathbf{E}, \quad (9)$$

$$\mathbf{B} = \mu \mathbf{H}. \quad (10)$$

We define the electric permittivity of the medium in terms of  $\mathbf{E}$  by

$$\varepsilon = \varepsilon(\mathbf{E}) = \varepsilon_0 (1 + \chi_1 + \chi_3 \|\mathbf{E}\|^2), \quad (11)$$

and we have

$$\mathbf{D} = \mathbf{D}(\mathbf{E}) = \varepsilon(\mathbf{E}) \mathbf{E}. \quad (12)$$

We recall that the refraction index of the medium is defined as

$$n = \frac{c_0}{c} = \sqrt{\frac{\varepsilon \mu}{\varepsilon_0 \mu}}, \quad (13)$$

where  $c_0$  is the speed of light in vacuum and  $c$  is the speed of light in the underlying medium. Using hypothesis 1 and expression (11) we obtain

$$n = n(\mathbf{E}) = \sqrt{1 + \chi_1 + \chi_3 \|\mathbf{E}\|^2}. \quad (14)$$

Let  $n_L = \sqrt{1 + \chi_1}$  be the linear refraction index; we have

$$n = n_L \sqrt{1 + \frac{\chi_3 \|\mathbf{E}\|^2}{n_L^2}}. \quad (15)$$

Since  $\chi_3 \ll n_L^2$  (see [Bet09]) we can perform a Taylor development up to the second order,

which yields to

$$n \approx n_L + \frac{\chi_3}{2n_L} \|\mathbf{E}\|^2 = n_L + n_2(\mathbf{E}). \quad (16)$$

The nonlinear index can be approximately defined as the sum of a zeroth order (constant) and a second order index which depends on the magnitude of  $\mathbf{E}$ , keeping in mind that nonlinear effects exist when this magnitude is very large.

The induction  $\mathbf{D}$  and the field  $\mathbf{E}$  are linked through the constitutive law (9) which is a nonlinear application (12) and, in the sequel, we will need to know the Jacobian matrix of this application, that we denote  $\mathcal{J}$ , and that we will derive, as well as its inverse, in any space dimension.

## 2.1 Derivation of the matrix $\mathcal{J}$

Let

$$\mathcal{J} = \mathcal{J}(\mathbf{E}) = \frac{\partial \mathbf{D}}{\partial \mathbf{E}}.$$

Using the constitutive law (9) we obtain

$$\mathcal{J} = \frac{\partial \varepsilon}{\partial \mathbf{E}} \mathbf{E} + \varepsilon \mathbf{I}_d, \quad (17)$$

where  $d$  is the dimension of  $\mathbf{E}$ ,  $\mathbf{I}_d$  is the identity matrix of  $\mathbb{R}^d$  and  $\varepsilon$  is given by (11). Let  $\alpha = 2\varepsilon_0\chi_3$ ; we have

$$\frac{\partial \varepsilon}{\partial E_j} = \alpha E_j, \quad j = 1 \dots d,$$

and  $\mathcal{J}$  writes as

$$\mathcal{J} = \alpha \mathbf{E} \otimes \mathbf{E} + \varepsilon \mathbf{I}_d. \quad (18)$$

For  $d = 3$ , the tensorial product of two vectors  $\mathbf{U}$  and  $\mathbf{V}$  is given by

$$\mathbf{U} \otimes \mathbf{V} = \begin{bmatrix} U_x V_x & U_x V_y & U_x V_z \\ U_y V_x & U_y V_y & U_y V_z \\ U_z V_x & U_z V_y & U_z V_z \end{bmatrix}. \quad (19)$$

For  $d < 3$ , the tensorial product is the minor of rank  $d$  of (19) associated to the selected variables.

**Proposition 1.**  $\mathcal{J}$  is a symmetric positive definite matrix.

**Proof 1.** We compute the determinant  $|\mathcal{J}|$  and obtain

$$|\mathcal{J}| = \varepsilon^{d-1} (\varepsilon + \alpha \|\mathbf{E}\|^2) \quad (20)$$

Since  $\alpha \geq 0$  and  $\varepsilon(\mathbf{E}) > 0 \forall \mathbf{E}$  we deduce that  $\mathcal{J}$  is invertible and we have

$$\mathcal{J}^{-1} = |\mathcal{J}|^{-1} \left( \alpha \varepsilon^{d-2} (\|\mathbf{E}\|^2 \mathbf{I}_d - \mathbf{E} \otimes \mathbf{E}) + \varepsilon^{d-1} \mathbf{I}_d \right) \quad (21)$$

$\mathcal{J}$  is a positive matrix if for any  $\mathbf{E} \neq 0$  we have  $\mathbf{E}^T \mathcal{J} \mathbf{E} > 0$ . We obtain

$$\mathbf{E}^T \mathcal{J} \mathbf{E} = \varepsilon_0(\chi_1 + 1) \|\mathbf{E}\|^2 + (\varepsilon_0\chi_3 + \alpha) \|\mathbf{E}\|^4 > 0. \quad (22)$$

All the formulas giving  $J$ , its determinant and its inverse are valid for any space dimension  $d$  and thus, for any number of components of  $\mathbf{E}$ . In the sequel, we focus on the case  $d = 1$  for which all the above-mentioned quantities are scalars. We denote by  $E$  the nonzero component of  $\mathbf{E}$  (without specifying which component is actually concerned), and we inject this quantity in Eq. (18), (20) and (21) to obtain

$$\begin{cases} \mathbf{E} \otimes \mathbf{E} &= E^2, \\ \mathcal{J} &= |\mathcal{J}| = \alpha E^2 + \varepsilon, \\ \mathcal{J}^{-1} &= \frac{1}{\alpha E^2 + \varepsilon}. \end{cases} \quad (23)$$

We can also replace the partial derivatives of  $\mathbf{E}$  by those of  $\mathbf{D}$  by using the chain rule formula

$$\frac{\partial \mathbf{D}}{\partial \xi} = \frac{\partial D(\mathbf{E})}{\partial \mathbf{E}} \frac{\partial \mathbf{E}}{\partial \xi} = \mathcal{J} \frac{\partial \mathbf{E}}{\partial \xi}, \quad (24)$$

where  $\xi$  stands for any variable on which  $\mathbf{D}$  and  $\mathbf{E}$  depend.  $\mathcal{J}^{-1}$  being well defined for all  $\mathbf{E}$ , the reciprocal formula of (24) writes

$$\boxed{\frac{\partial \mathbf{E}}{\partial \xi} = \mathcal{J}^{-1} \frac{\partial \mathbf{D}}{\partial \xi}} \quad (25)$$

Moreover, the fields  $\mathbf{B}$  et  $\mathbf{H}$  being linearly linked, by Eq. (10) we have

$$\boxed{\frac{\partial \mathbf{H}}{\partial \xi} = \mu^{-1} \frac{\partial \mathbf{B}}{\partial \xi}} \quad (26)$$

**Remark 2.**

If  $\chi_3 = 0$  then the medium is always linear whatever the magnitude of the electric field and  $\mathcal{J} = \varepsilon \mathbf{I}_d$  where  $\varepsilon$  is constant.

## 2.2 1d system

We assume that the fields only depend on the variable  $x$  and that  $B_z$  and  $E_y$  are zero. We also assume that, if they are any, currents are known and are not conducting. Then the system of Maxwell equations (1) simplifies to a system involving two equations that we write with  $D = D_z$ ,  $E = E_z$ ,  $J = J_z$ ,  $B = B_y$ , and  $H = H_y$

$$\begin{cases} \frac{\partial D}{\partial t} - \frac{\partial H}{\partial x} &= J, \\ \frac{\partial B}{\partial t} - \frac{\partial E}{\partial x} &= 0. \end{cases} \quad (27)$$

We define

$$\mathbf{Q} = (D, B)^T, \quad \mathcal{F}(\mathbf{Q}) = (H, E)^T, \quad \mathbf{J} = (J, 0)^T,$$

and system (27) writes under conservative form

$$\frac{\partial \mathbf{Q}}{\partial t} + \frac{\partial \mathcal{F}(\mathbf{Q})}{\partial x} = \mathbf{J}. \quad (28)$$

Using

$$\mathcal{A} = \frac{\partial \mathcal{F}}{\partial \mathbf{Q}} = - \begin{pmatrix} 0 & \mu^{-1} \\ \mathcal{J}^{-1} & 0 \end{pmatrix}, \quad (29)$$

where  $\mathcal{J}$  is here a scalar function which writes

$$\mathcal{J} = \varepsilon_0(1 + \chi_1 + 3\chi_3 E^2), \quad (30)$$

and we obtain the quasi-linear system

$$\frac{\partial \mathbf{Q}}{\partial t} + \mathcal{A} \frac{\partial \mathbf{Q}}{\partial x} = \mathbf{J}. \quad (31)$$

The matrix  $\mathcal{A}$  has two real and distinct eigenvalues and two associated eigenvectors

$$\begin{cases} \lambda_{1,2} &= \pm \frac{1}{\sqrt{\mu \mathcal{J}}}, \\ \mathbf{r}_k &= (1, -\mu \lambda_k)^T, \quad k = 1, 2. \end{cases} \quad (32)$$

We deduce that system (31) is strictly hyperbolic. The properties of the physical fields associated to the eigenvalues are studied in annex A.

### 3 Discontinuous Galerkin (DG) method

We consider system (28) in terms of rescaled quantities (see annex B) but without changing the notations. The computational domain is defined as the interval  $I = [a, b] \subset \mathbb{R}$  that we subdivide in cells  $I_j$  of uniform size  $\Delta x$

$$I_j = [x_j, x_{j+1}], \quad x_j = j\Delta x, \quad j = 1, \dots, N.$$

We multiply (28) by a test function  $\psi$  belonging to a space  $\mathbf{V}_j$  and we integrate by parts over  $I_j$  to obtain

$$\int_{I_j} \frac{\partial \mathbf{Q}}{\partial t} \psi dx - \int_{I_j} \mathcal{F}(\mathbf{Q}) \frac{\partial \psi}{\partial x} dx + \left[ \mathcal{F}(\mathbf{Q}) \psi \right]_{x_j}^{x_{j+1}} = \int_{I_j} \mathbf{J} \psi dx. \quad (33)$$

The space  $\mathbf{V}_j$  is chosen to be the set of polynomials of degree  $\leq n$  on  $I_j$  and we denote by  $u^j$  the projection of a function  $u$  on  $\mathbf{V}_j$

$$u^j(x, t) = \sum_{i=1}^{n+1} u_i^j(t) \psi_i^j(x). \quad (34)$$

System (33) writes

$$\int_{I_j} \frac{\partial \mathbf{Q}^j}{\partial t} \psi_k^j dx - \int_{I_j} \mathcal{F}(\mathbf{Q}^j) \frac{\partial \psi_k^j}{\partial x} dx + \left[ \tilde{\mathcal{F}}(\mathbf{Q}) \psi_k^j \right]_{x_j}^{x_{j+1}} = \int_{I_j} \mathbf{J}^j \psi_k^j dx, \quad k = 1, \dots, n+1, \quad (35)$$

where  $\tilde{\mathcal{F}}$  is an approximation of the continuous flux function  $\mathcal{F}$  at the boundaries of  $I_j$

$$\begin{aligned} \tilde{\mathcal{F}}(\mathbf{Q})(x_j) &= \Phi(\mathbf{Q}^{j-1}, \mathbf{Q}^j) = \Phi_{j-1,j}, \\ \tilde{\mathcal{F}}(\mathbf{Q})(x_{j+1}) &= \Phi(\mathbf{Q}^j, \mathbf{Q}^{j+1}) = \Phi_{j,j+1}, \end{aligned}$$

$\Phi$  is a numerical flux function which satisfy the consistency property (see [LHvL83])

$$\Phi(\mathbf{u}, \mathbf{u}) = \mathcal{F}(\mathbf{u}). \quad (36)$$

Several options exist for the definition of the numerical flux function  $\Phi$  verifying (36) and we choose here the local form of the Lax-Friedrichs flux defined by

$$\begin{aligned} \Phi(\mathbf{u}, \mathbf{v}) &= \frac{1}{2} \left( \mathcal{F}(\mathbf{u}) + \mathcal{F}(\mathbf{v}) - \frac{1}{2} C(\mathbf{u}, \mathbf{v})(\mathbf{v} - \mathbf{u}) \right), \\ C(\mathbf{u}, \mathbf{v}) &= \max_k (|\lambda_k(\mathbf{u})|, |\lambda_k(\mathbf{v})|), \end{aligned} \quad (37)$$

where the eigenvalues  $\lambda_k$  are given by (32). Then, system (35) writes as

$$\int_{I_j} \frac{\partial \mathbf{Q}^j}{\partial t} \psi_k^j dx - \int_{I_j} \mathcal{F}(\mathbf{Q}^j) \frac{\partial \psi_k^j}{\partial x} dx + \Phi_{j,j+1} \psi_k^j(x_{j+1}) - \Phi_{j-1,j} \psi_k^j(x_j) = \int_{I_j} \mathbf{J}^j \psi_k^j dx. \quad (38)$$

**Remark 3.** If the current source is a Dirac distribution in the spatial variable  $x$ , the polynomial projection (34) is not used and the RHS of (33) becomes

$$\int_{I_j} \mathbf{J}(x, t) \psi(x) dx = \int_{I_j} f(t) \delta_{x_0}(x) \psi(x) dx = f(t) \psi(x_0).$$

This formulation will be used for simulations involving a dipolar source in section 7.4.

It remains to choose the polynomial basis functions to finalize the formulation of the discrete equations of system (38). We consider two possibilities: the *nodal* basis spanned by the Lagrange polynomials and the *modal* basis spanned by the Bernstein polynomials.

### 3.1 Reference element

We choose as the reference element the unit interval  $\hat{I} = [0, 1]$  and we introduce a set of points that we call *nodes* forming the so-called Lagrange *mesh* of degree  $n$

$$\mathcal{T}_n = \{n_k \in \hat{I} : n_k = \frac{k-1}{n}, k = 1, \dots, n+1\}. \quad (39)$$

The Lagrange polynomials  $L_k$  of degree  $n$  are defined in unique way by the relation

$$L_k(n_m) = \delta_{km}, \quad \delta_{km} := \text{Kronecker's symbol}.$$

Let  $m = (m_1, m_2) \in \mathbb{N}^2$  such that  $m_1 + m_2 = n$ . The Bernstein polynomials of degree  $n$  are defined on  $\hat{I}$  by

$$B_m(x) = \frac{n!}{m_1!m_2!} x^{m_1} (1-x)^{m_2}.$$

Each local polynomial  $\psi_k^j$  defined on  $I_j = [x_j, x_{j+1}]$  as a unique image  $\hat{\psi}_k$  on the reference element  $I$

$$\hat{\psi}_k = \psi_k^j \circ \hat{F}_j, \quad (40)$$

where the affine application  $\hat{F}_j : \hat{I} \mapsto I_j$  writes

$$\hat{F}_j(\hat{x}) = (x_{j+1} - x_j)\hat{x} + x_j. \quad (41)$$

We deduce

$$\psi_k^j(x_j) = \hat{\psi}_k(0), \quad \psi_k^j(x_{j+1}) = \hat{\psi}_k(1). \quad (42)$$

Here  $\hat{\psi}_k$  stands for Lagrange or Bernstein polynomials for which a suitable numbering leads to the following relations

$$\boxed{\begin{aligned} \hat{\psi}_1(0) &= 1; \quad \hat{\psi}_k(0) = 0, \quad k = 2, \dots, n \\ \hat{\psi}_n(1) &= 1; \quad \hat{\psi}_k(1) = 0, \quad k = 1, \dots, n-1 \end{aligned}} \quad (43)$$

Injecting (42) in (38) we obtain

$$\boxed{\int_{I_j} \frac{\partial \mathbf{Q}^j}{\partial t} \psi_k^j dx - \int_{I_j} \mathcal{F}(\mathbf{Q}^j) \frac{\partial \psi_k^j}{\partial x} dx + \Phi_{j,j+1} \hat{\psi}_k(1) - \Phi_{j-1,j} \hat{\psi}_k(0) = 0} \quad (44)$$

### 3.2 Limited polynomials

To prevent spurious oscillations that may occur in the presence of singularities, we use the limitation process suggested in [Shu13, p. 547] where the limited polynomial  $\tilde{p}^j(x)$  is defined as follows

$$\begin{aligned} \tilde{p}^j(x) &= \theta_j(p^j(x) - \bar{u}^j) + \bar{u}^j, \\ \theta_j &= \min \left\{ \left| \frac{M - \bar{u}^j}{M_j - \bar{u}^j} \right|, \left| \frac{m - \bar{u}^j}{m_j - \bar{u}^j} \right|, 1 \right\}, \\ \bar{u}^j &= \frac{1}{dx} \int_{I_j} p^j(x) dx, \\ M_j &= \max_{x \in S_j} p^j(x), \quad m_j = \min_{x \in S_j} p^j(x), \end{aligned} \quad (45)$$

where  $p^j$  is the computed discrete solution on  $I_j$  at each time-step,  $M$  and  $m$  are respectively the maximum and the minimum values of the initial solution, and  $S_j$  is a set of quadrature points of the element  $I_j$ .

### 3.3 Finite volume method (FVM)

We can consider that a finite volume formulation is obtained from the discontinuous Galerkin formulation when the polynomial degree is set to 0. Then, with  $\psi^j = 1, \forall j$  the projection

formula (34) becomes

$$\mathbf{Q}^j(x, t) = \mathbf{Q}_1^j(t). \quad (46)$$

Neglecting the subscript 1 and setting  $\mathbf{J} = 0$ , system (44) writes

$$\frac{\partial \mathbf{Q}^j}{\partial t} \Delta x + \Phi(\mathbf{Q}^j, \mathbf{Q}^{j+1}) - \Phi(\mathbf{Q}^{j-1}, \mathbf{Q}^j) = 0 \quad (47)$$

The finite volume scheme given by (47) is only first order accurate in space independently of the chosen numerical flux. To increase the spatial accuracy we use the MUSCL [Lee79] method which may be summarized as follows

1- In each element  $I_j$  define left, right and central slopes by

$$p_l^j = \frac{1}{\Delta x}(u^j - u^{j-1}), \quad p_r^j = \frac{1}{\Delta x}(u^{j+1} - u^j), \quad p_c^j = \frac{1}{2\Delta x}(u^{j+1} - u^{j-1}). \quad (48)$$

2- Use a slope limitation technique such as the *minmod* limiter [Lee79]

$$p_{\text{lim}}^j = \text{minmod}(p_l^j, p_r^j, p_c^j), \quad (49)$$

where  $\text{minmod}(a, b, c) = \max(|a|, |b|, |c|)$  if  $a, b$  and  $c$  have all the same sign and 0 otherwise.

3- Compute new values at boundaries of  $I_j$

$$u_{\text{lim}}^{j,+} = u^j + \frac{\Delta x}{2} p_{\text{lim}}^j, \quad (50)$$

$$u_{\text{lim}}^{j+1,-} = u^{j+1} - \frac{\Delta x}{2} p_{\text{lim}}^j. \quad (51)$$

Applying the process to each component of  $\mathbf{Q}$ , the finite volume scheme (47) becomes

$$\frac{\partial \mathbf{Q}^j}{\partial t} \Delta x + \Phi(\mathbf{Q}_{\text{lim}}^{j+1,-}, \mathbf{Q}_{\text{lim}}^{j+1,+}) - \Phi(\mathbf{Q}_{\text{lim}}^{j,-}, \mathbf{Q}_{\text{lim}}^{j,+}) = 0 \quad (52)$$

## 4 Runge-Kutta scheme

We rewrite the semi-discrete systems (44) and (47) as

$$\mathbf{Q}_j^{n+1} = \mathbf{Q}_j^n + \Delta t \mathcal{R}(\mathbf{Q}^n),$$

which is time-integrated using a Runge-Kutta (RK) scheme of order  $k$

$$\begin{cases} \mathbf{Q}^{(0)} &= \mathbf{Q}^n, \\ \mathbf{Q}^{(i)} &= \sum_{j=0}^{i-1} (\alpha_{i,j} \mathbf{Q}^{(j)} + \beta_{i,j} \Delta t \mathcal{R}(\mathbf{Q}^{(j)})), \quad i = 1, \dots, k, \\ \mathbf{Q}^{n+1} &= \mathbf{Q}^{(k)}, \end{cases} \quad (53)$$

with

$$\sum_{j=0}^{i-1} \alpha_{i,j} = 1.$$

We will call Runge-Kutta method, the classical method obtained with the coefficients  $\alpha_{i,j}$  and  $\beta_{i,j}$  defined for  $j = 0 \dots, i-1$  et  $i = 1 \dots, k$  by

$$\begin{aligned} \alpha_{i,j} &= \delta_{i,j}, \\ \beta_{i,j} &= \frac{\delta_{i,j}}{k+1-i}, \end{aligned} \quad (54)$$

where  $\delta_{i,j}$  is the Kronecker's symbol. The time step  $\Delta t$  is determined by the relation

$$\Delta t = \frac{\Delta x}{c_0} \text{CFL},$$

where  $c_0$  is the speed of light in vacuum (which is the maximal speed of electromagnetic waves) and the Courant number CFL is a positive real number resulting from an appropriate linear stability analysis. In [CS01], the authors propose to use a Runge-Kutta method of order  $n+1$  for spatial polynomials of degree  $\leq n$  with a Courant number given by

$$\text{CFL} = \frac{1}{2p+1}. \quad (55)$$

This method happens to be expensive in terms of CPU time and, as an alternative, we will use the third order scheme given in [Got05] which writes under the form (53) with  $k=3$  and with coefficients that write in matricial form as

$$\alpha = \begin{pmatrix} 1 & 0 & 0 \\ \frac{3}{4} & \frac{1}{4} & 0 \\ \frac{1}{3} & 0 & \frac{2}{3} \end{pmatrix} \quad \beta = \begin{pmatrix} 1 & 0 & 0 \\ 0 & \frac{1}{4} & 0 \\ 0 & 0 & \frac{2}{3} \end{pmatrix}. \quad (56)$$

We will refer to this scheme as OS3 to distinguish it from the classical RK3 Runge-Kutta scheme.

## 5 Approximation of the E field

The Runge-Kutta scheme yields the inductions  $D^{n+1}$  and  $B^{n+1}$  from  $D^n$  and  $B^n$  but the numerical flux function (37) depends on  $E^n$  and  $H^n$  and, while the latter is obtained from  $B^n$  thanks of a simple division by  $\mu_r$ , in order to obtain  $E^n$  from  $D^n$  one has either to directly invert the electric constitutive law (9) or make use of a specific procedure to avoid this (costly) direct inversion. We present here three strategies for computing  $E$ , the first two compute approximate roots of the cubic equation (9) and the third one solves the differential equation (25) (with  $\xi = t$ ).



### 5.1 Newton method

The field  $D^n$  being known, we want to evaluate  $E^n$  such that  $D^n \approx \varepsilon_r(E^n)E^n$  where  $\varepsilon_r(E) = \varepsilon_{L,r} + \chi_3 E^2$ . In order to do so, we define  $G(E) = \varepsilon_r(E)E - D^n$  and we look for the zeros of  $G$  using Newton's method

$$E^{(0)} = E^{n-1} ; \quad E^{(k+1)} = E^{(k)} - \frac{G(E^{(k)})}{G'(E^{(k)})}, \quad k \geq 0.$$

Note that Newton's method works iff  $G'(E^{(k)}) \neq 0$ , which is always true in the present case since  $\chi_3 \geq 0$  and when  $\chi_3 < 0$  we assume that the nonlinear term of  $G'(E)$  is small compared to the linear permittivity  $\varepsilon_{L,r}$ .

### 5.2 Padé Approximants

Another way to approximate solutions of equation (9) is with Padé approximants [O<sup>+</sup>10] which, in the case of a purely Kerr material, lead to

$$E^n = \left[ \frac{1 + \frac{2\chi_3}{\varepsilon_{L,r}^3}(D^n)^2}{1 + \frac{3\chi_3}{\varepsilon_{L,r}^3}(D^n)^2} \right] [\varepsilon_{L,r}]^{-1} D^n. \quad (57)$$

### 5.3 Euler method

Here, the method used to compute  $E$  relies on the time discretization of the relation

$$\frac{\partial D}{\partial t} = \mathcal{J}(E) \frac{\partial E}{\partial t}. \quad (58)$$

We set

$$\frac{\partial U}{\partial t} \approx \frac{U^n - U^{n-1}}{\Delta t},$$

and we approximate (58) by

$$D^n - D^{n-1} = \mathcal{J}(E^{n-1}) (E^n - E^{n-1}).$$

We deduce

$$\boxed{E^n = E^{n-1} + \mathcal{J}^{-1}(E^{n-1}) (D^n - D^{n-1})}. \quad (59)$$

We can remark that the Euler method corresponds to the (unlikely) case where, at each time step, Newton's method yields the desired result (i.e.  $G(E) = 0$ ) in one iteration. We would obtain in this case

$$E^n = E^{n-1} - \frac{G(E^{n-1})}{G'(E^{n-1})}, \quad G(E^n) = 0, \quad \forall n.$$

But  $G' = J$  and then

$$\begin{aligned} E^n &= E^{n-1} - \mathcal{J}^{-1}(E^{n-1}) (\varepsilon_r(E^{n-1})E^{n-1} - D^n) \\ &= E^{n-1} - \mathcal{J}^{-1}(E^{n-1}) (D^{n-1} - D^n), \end{aligned}$$

which is exactly Eq. (59). We may conclude that the Euler method is much less accurate than Newton's method but the latter is, on one hand, more expensive and, on the other hand, imposes conditions on  $\chi_3$  and/or on  $\mathcal{J}$  such that  $G'(E) \neq 0, \forall E$ . We note that all three methods for computing  $\mathbf{E}$  extend easily to higher spatial dimensions.

## 6 Electromagnetic energy

In the absence of electric charge and current densities, the conservation law of the electromagnetic energy writes in differential form [Jac99, p. 237]) as

$$\frac{\partial u}{\partial t} + \nabla \cdot \mathbf{S} = 0, \quad (60)$$

where  $u = \frac{1}{2}(\mathbf{E} \cdot \mathbf{D} + \mathbf{B} \cdot \mathbf{H})$  is the electromagnetic energy density and  $\mathbf{S} = \mathbf{E} \times \mathbf{H}$  is the Poynting vector. The integral form of this conservation law is given by

$$\frac{\partial}{\partial t} \int_V u dV + \int_{\partial V} \mathbf{S} \cdot \mathbf{n} ds = 0, \quad (61)$$

where  $V$  is an arbitray volume and  $\mathbf{n}$  is the outward unit normal vector. The above expression of the conservation law of the electromagnetic energy also known as *Poynting's theorem* is only valid for linear and non-dispersive materials. For nonlinear materials, Sjöberg [Sjö07] proposes to replace the Poynting equation 60 by the inequality

$$\frac{\partial u}{\partial t} + \nabla \cdot \mathbf{S} \leq 0, \quad (62)$$

where the electromagnetic energy density  $u$  in the one dimensional spatial case writes as

$$u = \frac{1}{2}BH + ED(E) - \int_0^E D(E')dE'. \quad (63)$$

For Kerr materials, the (63) leads to

$$\begin{aligned} u &= \frac{1}{2}(BH + \varepsilon_{L,r}E^2) + \frac{3}{4}\chi_3E^4, \\ &= u_L + \frac{3}{4}\chi_3E^4, \end{aligned} \quad (64)$$

where  $u_L$  has the same definition as in the linear case. Thus we will use  $u$  given by (64) for both linear and nonlinear materials to check the conservation law of energy.

## 7 Numerical experiments

We have selected four test problems corresponding to the propagation of a square-shaped pulse, a gaussian pulse, a wave packet, and to the the radiation of an oscillating electric dipole. The propagation or radiation takes place in an infinite medium which is either the air or the vacuum. Table 1 below summarizes the electromagnetic parameters playing a role in this numerical study. We note that the magnitude of the incident electric field must

be very large to obtain noticeable nonlinear effects. In particular, in the case of vacuum, the magnitude must be greater than  $10^{13}$  V/m whereas a magnitude of  $10^6$  V/m is sufficient in the case of the air as will be seen below.

Mediaum	$\varepsilon_{L,r}$	$\chi_3$
Air	1.0003	$3.675 \times 10^{-13} \text{ m}^2/\text{V}^2$
Vacuum	1.0	$7.195 \times 10^{-29} \text{ m}^2/\text{V}^2$

Table 1: Linear permittivity and third order nonlinear susceptibility.

## 7.1 Square-shaped pulse

We consider the propagation of a square-shaped pulse in the air. The magnitude of the pulse is set to 1 V/m. The computational domain is the interval  $I = [-1, 1]$  and we define the square-shaped pulse as the characteristic function of the interval  $[a, b] \subset I$

$$\mathbf{1}_{[a,b]}(x) = \begin{cases} 1 & \text{if } x \in [a, b], \\ 0 & \text{otherwise.} \end{cases}$$

We set  $[a, b] = [-\frac{3}{4}, -\frac{1}{4}]$  and we discretize the domain with 100 elements. We select the RK1 time integration scheme in combination with the first order FV scheme, and the OS3 time integration scheme in combination with the DG scheme. We show on figure 1 the distribution of  $E_z$  obtained at  $t = 2.5$  ns with the first order FV and DG- $\mathbb{P}_1$  methods together with the exact solution.

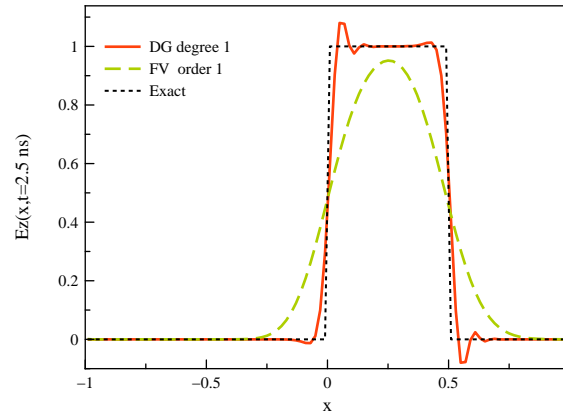


Figure 1: First order FV and DG- $\mathbb{P}_1$  methods.

We now increase the spatial accuracy of the FV scheme using the MUSCL technique with slope limiters (3.3) and that of the DG scheme by considering a third order interpolation degree. The OS3 time integration scheme is adopted in both cases. Figure 2 shows the obtained solutions at  $t = 0.3$  ns. We observe spurious oscillations when the FV method is used without limiters, whereas when the latter are activated the FV solution compares

well with the DG- $\mathbb{P}_3$  one and with the exact solution albeit the numerical diffusion is more pronounced in the case of the FV method with limiters.

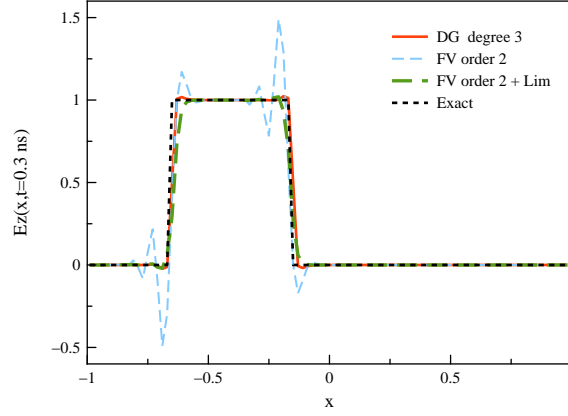


Figure 2: Second order FV and DG- $\mathbb{P}_3$  methods.

The DG- $\mathbb{P}_3$  method also exhibits some slight oscillations but the latter are damped and almost disappear when the interpolation degree is increased as can be seen on figure 3.

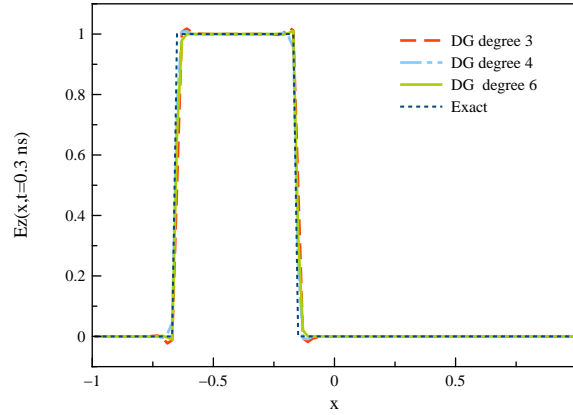


Figure 3: DG method with order 3, 4 and 6.

In order to be able to make comparisons with the exact solution in the nonlinear case, we have to regularize the characteristic function  $1_{[a,b]}(x)$  because the procedure described in section C and taken from [PNTB09] requires  $C^1$  initial functions. In order to do so, we introduce the sequence of functions defined by

$$\phi_{[a,b]}^k(x) = \frac{1}{1 + e^{-2k(x-a)}} - \frac{1}{1 + e^{-2k(x-b)}}.$$

We show on figure 4 the characteristic function  $1_{[a,b]}(x)$  on the interval  $[-\frac{3}{4}, -\frac{1}{4}]$  together

with two terms of the sequence  $\phi_{[a,b]}^k$  and we see that the term  $\phi_{[a,b]}^{40}$  is a good approximation of the characteristic function. Thus, in the following, we will use the function  $\phi_{[a,b]}^{40}$  for the initialization of the  $E$  field.

Figure 5 shows the exact solution and the approximate solutions resulting from the second order FV method with limiters and the DG- $\mathbb{P}_1$  method, at  $t = 2.5$  ns computed on a mesh with 300 elements. We have adopted the RK2 time integration scheme. The magnitude  $E_0$  of the initial field has been set to  $10^3$  V/m. We note that the wave is transported without deformation as in a perfectly linear medium keeping in mind that the target solution being regular, the FV and DG solutions are oscillations free. We also mention that the  $E_z$  component is computed at each Runge-Kutta method using Newton's method.

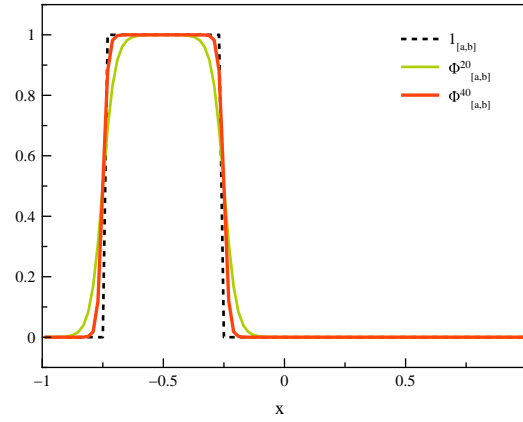


Figure 4: Regularized characteristic function.

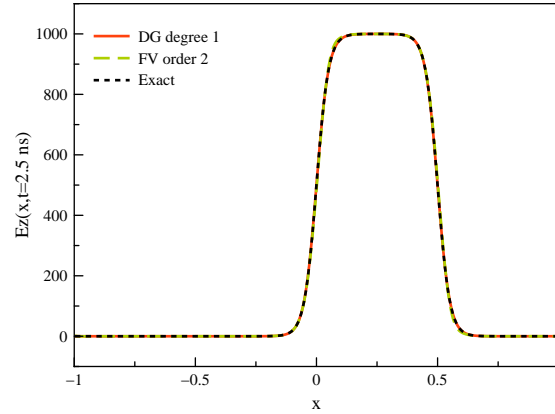


Figure 5: Second order FV and DG- $\mathbb{P}_1$  solutions for  $E_0 = 10^3$  V/m.

We use the same data as in the case of figure 5 except the magnitude of the initial field which is now set to  $10^6$  V/m. The corresponding results are shown on figure 6. The nonlinear

effects materialize as a discontinuity (shock wave) upstream of the front, and a rarefaction wave downstream of the front, but the magnitude of the field is conserved. The DG- $\mathbb{P}_1$  solution compares relatively well to the exact solution but the FV solution exhibits strong oscillations at the level of the shock discontinuity.

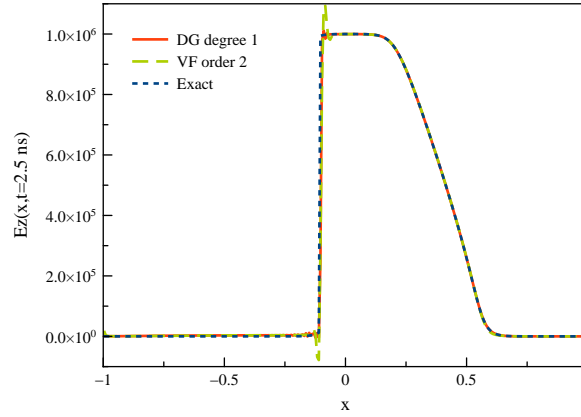


Figure 6: Second order FV and DG- $\mathbb{P}_1$  solutions for  $E_0 = 10^6$  V/m.

In order to damp the spurious oscillations of the FV solution we apply slope limiters. The corresponding results are shown on figure 7. We observe that the FV solution is almost monotone and the oscillations resulting from the DG- $\mathbb{P}_1$  method are more noticeable.

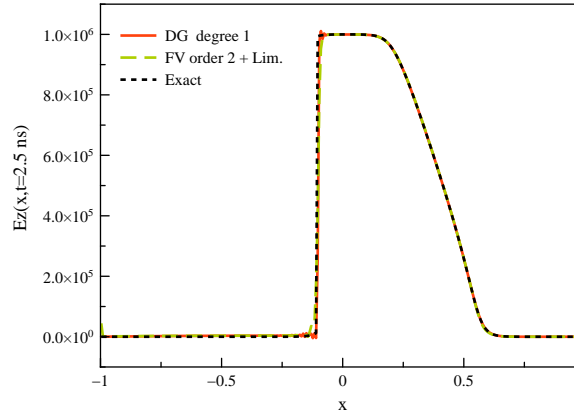


Figure 7: Second order FV with limiters and DG- $\mathbb{P}_1$  solutions for  $E_0 = 10^6$  V/m.

We now want to assess the role of the interpolation degree in the DG method. In doing so, we keep the simulation parameters unchanged and use the OS3 time integration scheme. The obtained solutions are shown on figure 8. We observe that the spurious oscillations appearing in the DG- $\mathbb{P}_1$  solution are damped when the interpolation degree is raised but

additional oscillations form upstream of the shock discontinuity. Moreover, the amplitude of these new oscillations increases with the interpolation degree.

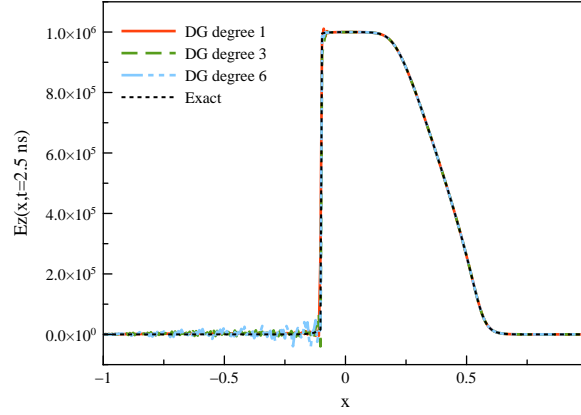


Figure 8: DG method with Lagrange polynomial of degree 1, 3 and 6.

Then, we apply the limiting procedure described in section 3.2. We see on the plots of figure 9 that the oscillations upstream of the shock discontinuity have almost disappeared while those existing at the level of the discontinuities are still present.

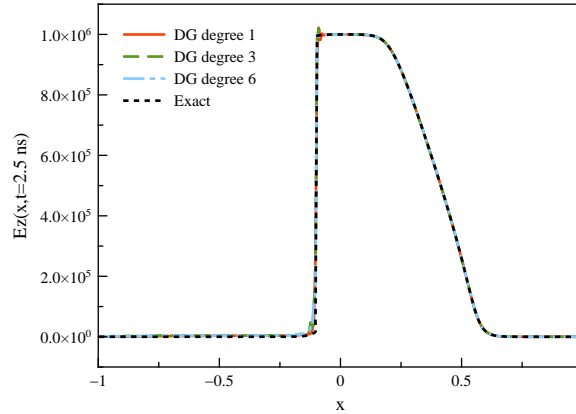


Figure 9: DG method with with Lagrange polynomials of degree 1, 3 and 6, and with limited polynomials.

We performed the same numerical experiments but using this time the Bernstein polynomials and without limiters (we recall that Lagrange and Bernstein polynomials are identical when the interpolation degree is equal to 1). The obtained results are plotted on figure 10. The graphs of figure 10 show that the limiters (3.2) almost fail in damping the oscillations. From now on, we will use Lagrange polynomials and the OS3 time integration scheme.

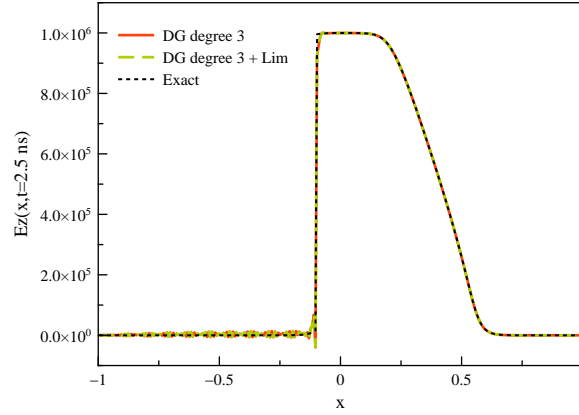


Figure 10: DG method with with Bernstein polynomial of degree 3, and with limited polynomials.

## 7.2 Gaussian pulse

This second test problem is concerned with the propagation of a Gaussian pulse. The initial profile of the the electric field component is given by

$$E(x, 0) = E_0(x) = A e^{-\frac{x^2}{2\sigma^2}}, \quad A = 10^6, \quad \sigma = 0.15.$$

The propagation domain is the interval  $I = [-1, 2]$  which is meshed using 300 equally sized elements. The initial profile is plotted on figure 11 together with the DG- $\mathbb{P}_3$  solutions at time  $t = 2.3$  ns respectively computed in vacuum and air (see table 1).

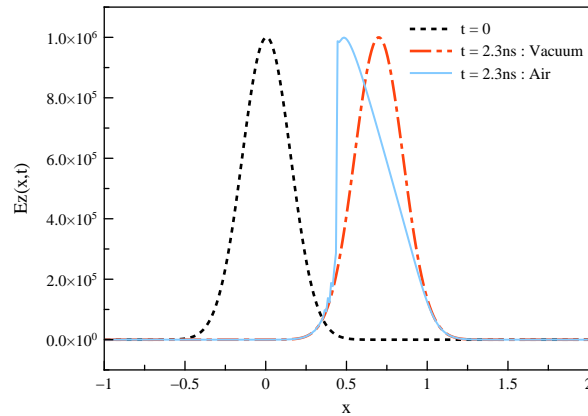


Figure 11: Propagation of a Gaussian pulse,  $A(\text{vacuum}) = A(\text{air}) = 10^6$  V/m.

We observe that when the magnitude is set to  $10^6$  V/m, the front propagates in vacuum



as in a linear medium whereas in the air a shock discontinuity is forming upstream of the pulse. We perform the same simulation in vacuum setting the magnitude to  $7.10^{13}$  V/m and we compare the obtained solution with that computed in the air with a magnitude set to  $10^6$  V/m (see figure 12). If we multiply the solution computed in the air by the ratio of the two initial magnitudes, the two solutions become almost identical and compare very well with the exact solution.

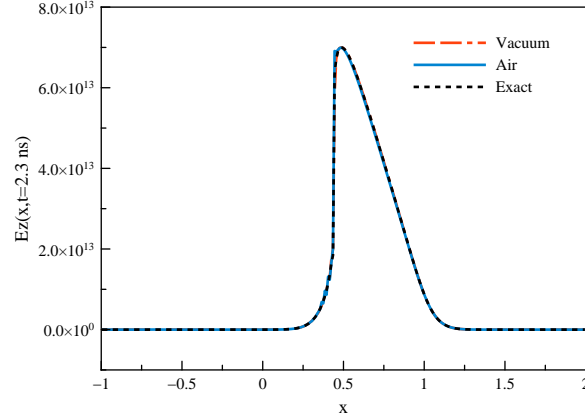


Figure 12: Propagation of a Gaussian pulse,  $A(\text{vacuum}) = 7.10^{13}$  V/m,  $A(\text{air}) = 10^6$  V/m.

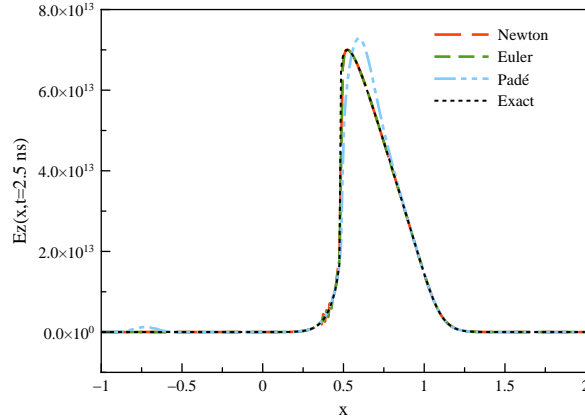


Figure 13: Euler and Padé approximants methods:  $A = 7.10^{13}$

We now simulate the propagation of the pulse in vacuum until  $t = 3.33$  ns. We see (figure 14) that slight oscillations appear near the shock discontinuity and these oscillations are not totally damped when we apply limiters neither when we increase the interpolation degree contrary to what has been observed for the square-shaped pulse. It should be noted that the shock occurs at time  $t = T_{\text{shock}} \leq T_{\text{max}}$  ns where  $T_{\text{max}}$  is computed from equation 92. In theory,  $T_{\text{max}}$  and  $T_{\text{shock}}$  are identical but in practice they differ according to the accuracy of

$T_{\max}$  given by 92.

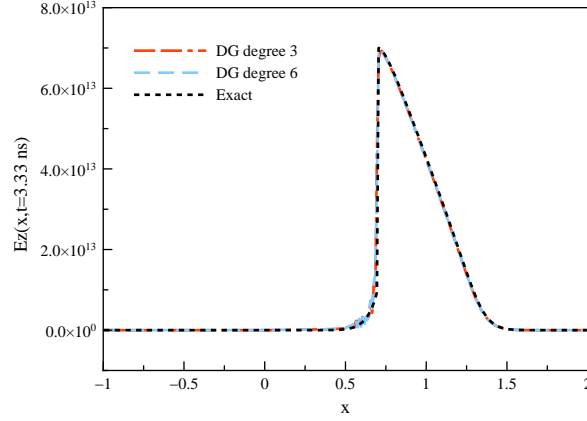


Figure 14: Propagation of a Gaussian pulse, DG- $\mathbb{P}_3$  and DG- $\mathbb{P}_6$  methods.

The energy computed using the DG- $\mathbb{P}_3$  method is shown on figure 15 where the time  $T_{\text{shock}}$  is also indicated. Here we have  $T_{\text{shock}} \approx T_{\max} = 2.3$  ns. For  $t > T_{\max}$  we observe a decay of the electromagnetic energy which is in accordance with the general conservation law 62. However the energy reduction being less than 1% the wave amplitude is almost unchanged.

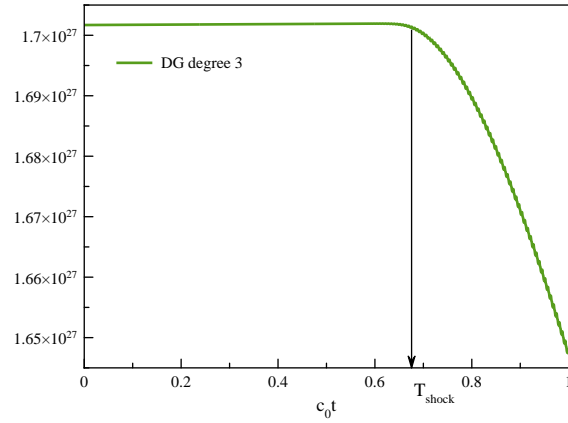


Figure 15: Electromagnetic energy: non linear medium

We want to check if the decay of energy is physical (i.e. dissipation process due to the shocks) or numerical. To do so, we use the same data as in the previous simulation but the magnitude of the electric field is now set to  $10^6$  V/m and we know that at this level of magnitude the vacuum behaves like a perfect linear medium. We can see on figure 16 that the energy is well conserved and it is unlikely that any numerical method becomes more dissipative in a nonlinear case than in a linear one.

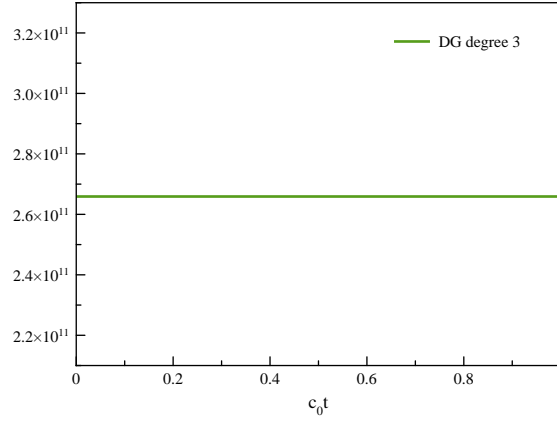
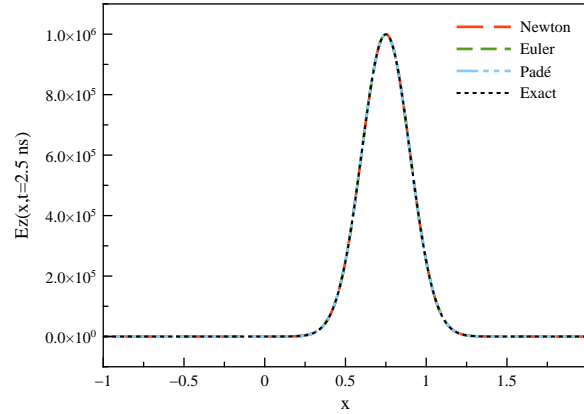
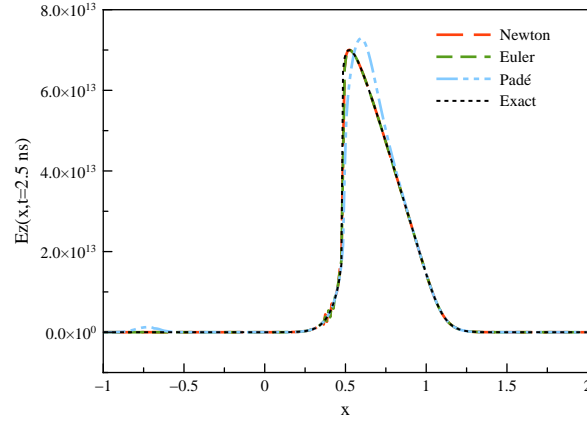


Figure 16: Electromagnetic energy: linear medium

Section (5) described three methods to compute the electric field  $E$  from the induction  $D$ . To compare them, we simulate the propagation of the gaussian pulse in vacuum with two distinct initial magnitudes for  $E$ . Figure 18 shows  $E$  at  $t = 2.5$  ns with an initial magnitude  $A = 10^6$  V/m. We can see that all approximated electric fields compare very favorably with the exact solution at this magnitude level, at which the medium behave like a perfectly linear material.

Figure 17: Newton, Euler and Padé approximants methods:  $A = 10^6$ 

With an initial magnitude  $A = 7.10^{13}$  V/m, however, the medium is non-linear and results obtained using Padé approximants lose accuracy compared to the two other methods, as can be seen in figure 13.

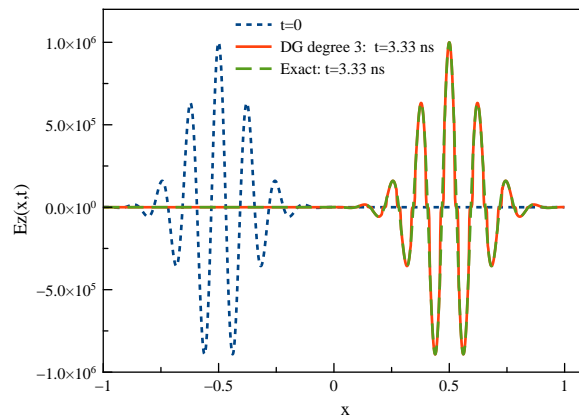
Figure 18: Newton, Euler and Padé approximants methods:  $A = 7.10^{13}$ 

### 7.3 Wave packet

We now consider the propagation of a wave packet given at initial time by

$$E_0(x) = A e^{-30(x-x_0)^2} \cos 2\pi f(x-x_0), \quad A = 10^6, \quad x_0 = -0.25 \text{ m}, \quad f = 8 \text{ GHz}. \quad (65)$$

We show on figure 19 the initial profile of the electric field and the solution obtained in vacuum at time  $t = 3.33 \text{ ns}$  using the DG- $\mathbb{P}_3$  method. We again observe that when the magnitude is set to  $10^6 \text{ V/m}$  the medium behaves as a linear medium and the front propagates with no deformation. The DG solution compares very well to the exact solution. When the medium is taken to be the air all the other parameters being unchanged, we obtain the solution shown on figure 20. A drastically different response is observed and, in particular, the magnitude of the signal is damped by almost 50%.

Figure 19: Propagation of a wave packet: initial profile and DG- $\mathbb{P}_3$  solution,  $A(\text{vacuum}) = 1.10^6 \text{ V/m}$ .

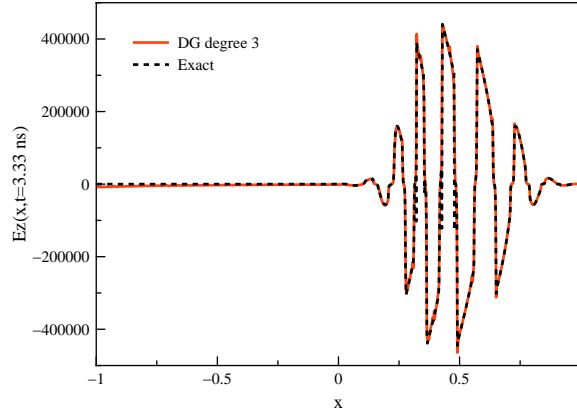


Figure 20: Propagation of a wave packet: initial profile and DG- $\mathbb{P}_3$  solution,  $A(\text{air}) = 1.10^6$  V/m.

Figure 21 shows the evolution of the discrete energy related to the last experiment. For  $t > T_{\text{shock}}$ , the energy decreases significantly while the field is yet entirely in the computational domain (see figure 20). Furthermore we can see that the reduction rate in energy is almost the same as for the electric field magnitude.

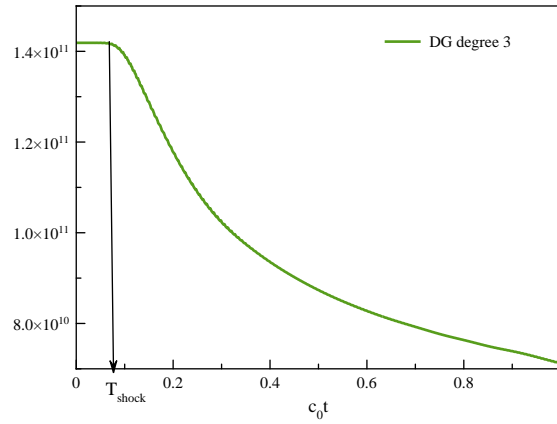


Figure 21: Propagation of a wave packet: electromagnetic energy.

Figure 22 shows the evolution of the wave packet energy at different frequencies and we can see that the decay is quite proportional to the frequency. This is most probably due to the number of shocks which also grows with the frequency.

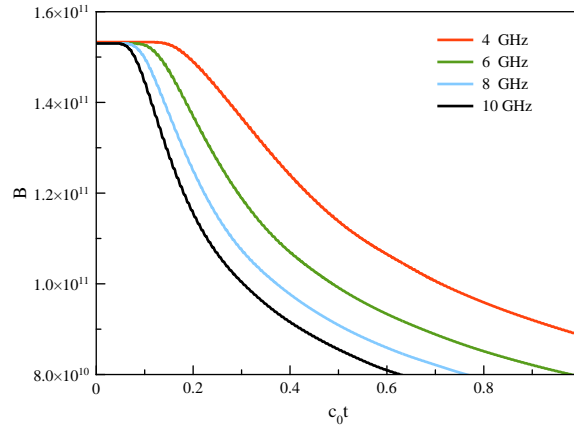


Figure 22: Decay of energy%frequency

## 7.4 Electric dipole radiation

We consider an oscillating electric dipole located at the center of the open domain  $I = ]-a, a[$ . We define the dipole through the induced current source

$$\mathbf{J}_z(x, t) = A e^{-10(t-t_0)^2} \sin(2\pi f t) \delta(x), \quad A = 10^6, \quad t_0 = 2 \text{ ns}. \quad (66)$$

where  $\delta(x)$  is the Dirac distribution. We emphasize that the initial electromagnetic field is set to zero and the absorbing boundary condition is approximated by means of an upwind scheme. We first place the dipole in the vacuum and since the electric field magnitude is only of  $10^6$  V/m the response of the medium is linear and the analytic solution is easily computable. Figures 23-24 show respectively plots of the solution at  $t = 5$  ns and the time evolution of the electric field at  $x = 0.15$  m induced by the dipole oscillating at 0.1 GHz. With this parameters, the wavelength is about 3 m and thus figure 24 shows the *near-field*. We can see that numerical and analytic solutions compare very well.

We carry out the same experiments with the dipole oscillating now with a frequency 1 GHz and plot the results on figures 25 and 26. We can notice that the numerical solutions compare very well to the exact ones thus we may also conclude that raising the frequency does not deteriorate the quality of the numerical solutions.

We now choose the air as the propagating medium and we carry out the same experiments as in vacuum but the air being nonlinear at this range of magnitude, we cannot compare to the analytic solution which is missing. Figures 27 and 28 show the numerical solutions with the dipole oscillating with frequency 0.1 GHz. The nonlinear effects result in a slight stiffening of the profile together with a decay in the magnitude of the electric field.

Figures 29 and 30 show the DG- $\mathbb{P}_3$  solutions computed with the dipole oscillating now with frequency 1 GHz. This relative high frequency results in multiple shocks and a large decay in the magnitude of the electric field. We may notice some spurious oscillations at shock locations (see figure 29) and on the right part of the figure 29, oscillations that were not observed in the wave packet test problem at higher frequencies. The main difference with the present test problem is that the frequency is also a factor (together with the magnitude)

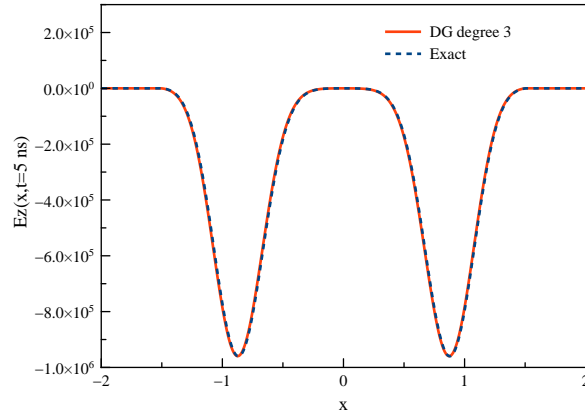


Figure 23: Radiating dipole: medium is vacuum,  $f = 0.1$  GHz :  $Ez(x, t = 5)$ .

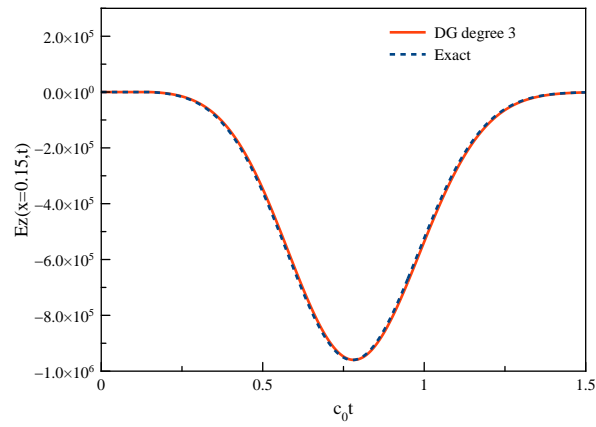


Figure 24: Radiating dipole: medium is vacuum,  $f = 0.1$  GHz :  $Ez(x = 0.15, t)$ .

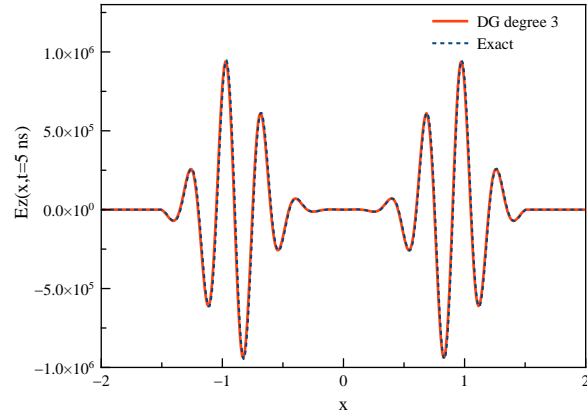


Figure 25: Radiating dipole: medium is vacuum,  $f = 1$  GHz :  $Ez(x, t = 5)$ .

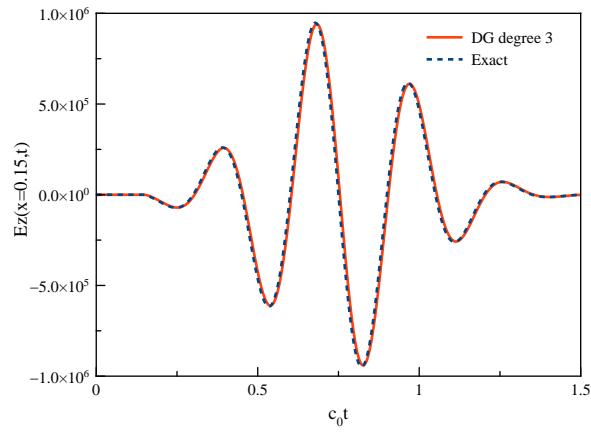


Figure 26: Radiating dipole: medium is vacuum,  $f = 1$  GHz :  $Ez(x = 0.15, t)$ .



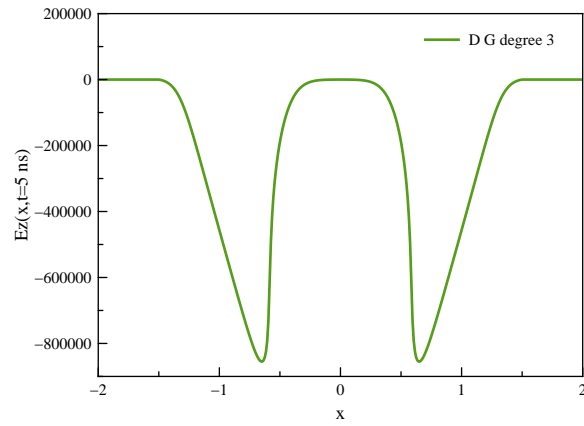


Figure 27: Radiating dipole: medium is air,  $f = 0.1 \text{ GHz}$  :  $E_z(x, t = 5)$ .

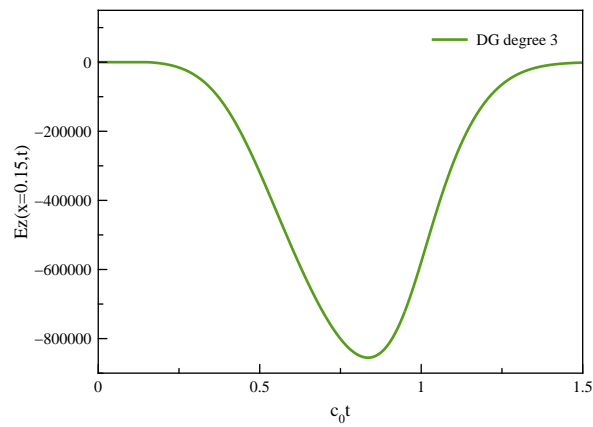


Figure 28: Radiating dipole: medium=air,  $f = 0.1 \text{ GHz}$  :  $E_z(x = 0.15, t)$ .

in the appearance of nonlinear effects while only the magnitude was decisive in the other experiments

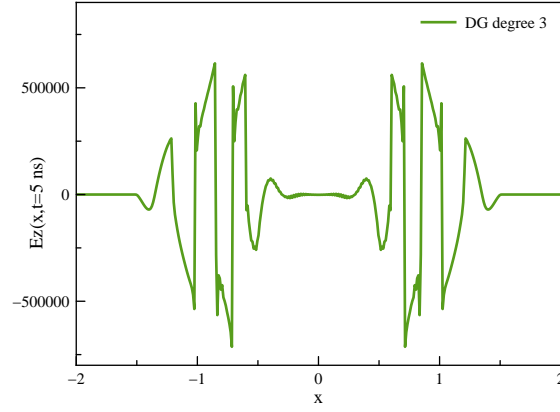


Figure 29: Radiating dipole: medium is air,  $f = 1$  GHz :  $Ez(x, t = 5)$ .

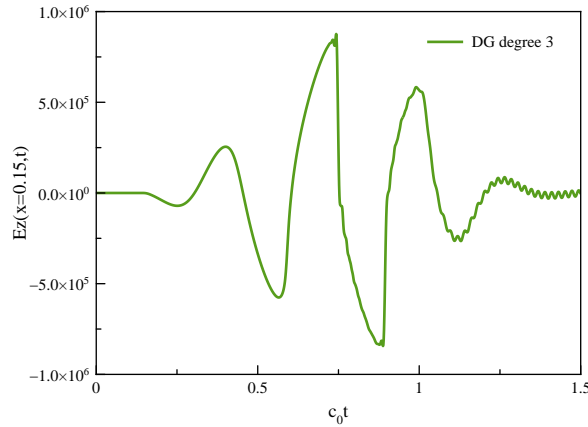


Figure 30: Radiating dipole: medium is air,  $f = 1$  GHz :  $Ez(x = 0.15, t)$ .

## 8 Conclusion

In this paper, we have presented the results of a preliminary study aiming at the numerical solution of the nonlinear Maxwell equations in 1d using discontinuous Galerkin methods. In doing so, we have used an upwind scheme and limitation techniques because they have a proven ability to capture shocks and other kinds of singularities in the fluid dynamics framework. The specific nature of nonlinear electrodynamics prompted the use of the Newton or Euler method to update electric fields from inductions. The numerical results presented here compare well to exact solutions where they are known, and this gives us confidence

towards extending this work to higher spatial dimensions.

## A Spectral analysis

### A.1 Eigenvalues and eigenvectors

In the following, we characterize the hyperbolic nature of the Maxwell-Kerr system by studying its eigenvalues and separating the associated eigenvectors in terms of *genuinely nonlinear* fields and *linearly degenerate* fields whose definitions are first recalled.

Let  $\mathbf{Q} = (Q_1, Q_2)^T$  and  $\nabla\lambda(\mathbf{Q}) = \left( \frac{\partial\lambda}{\partial Q_1}, \frac{\partial\lambda}{\partial Q_2} \right)^T$ .

**Definition 1.**

We say that the field associated to the eigenvalue  $\lambda$  is genuinely nonlinear if and only if

$$\nabla\lambda(\mathbf{Q}) \cdot \mathbf{r}(\mathbf{Q}) \neq 0 \quad \forall \mathbf{Q} \in \mathbb{R}^2, \quad (67)$$

where  $\mathbf{r}$  is the eigenvector associated to  $\lambda$ .

**Definition 2.**

We say that the field associated to the eigenvalue  $\lambda$  is linearly degenerated if and only if

$$\nabla\lambda(\mathbf{Q}) \cdot \mathbf{r}(\mathbf{Q}) = 0 \quad \forall \mathbf{Q} \in \mathbb{R}^2. \quad (68)$$

We recall that in the 1d case with  $\mathbf{Q} = (D, B)^T$  we have

$$\begin{cases} \lambda_{1,2} &= \pm \frac{1}{\sqrt{\mu\mathcal{J}}}, \\ \mathbf{r}_k &= (1, -\mu\lambda_k)^T, \quad k = 1, 2 \\ \mathcal{J} &= \varepsilon_0(1 + \chi_1 + 3\chi_3 E^2). \end{cases} \quad (69)$$

Then

$$\nabla\lambda_{1,2}(\mathbf{Q}) = \mp \left( 3\varepsilon_0\chi_3\mu^{-\frac{1}{2}}J^{-\frac{5}{2}}E \right) (1, 0)^T, \quad (70)$$

from which we deduce that

$$\nabla\lambda_{1,2} \cdot \mathbf{r}_{1,2} = \mp 3\varepsilon_0\chi_3\mu^{-\frac{1}{2}}J^{-\frac{5}{2}}E. \quad (71)$$

We recall that in the linear case  $\chi_3 = 0$  and all the fields are thus linearly degenerated. In the nonlinear case, the fields are genuinely nonlinear if  $E \neq 0$  and linearly degenerated if  $E = 0$ .

### A.2 Riemann invariants

**Definition 3.**

We call rank Riemann invariant, a function  $R \in \mathbb{C}^1$  such that

$$(\nabla R \cdot \mathbf{r})(\mathbf{Q}) = 0 \quad \forall \mathbf{Q}. \quad (72)$$

Such functions have the peculiarity of being constant on the characteristic curves defined by

$$\frac{dX}{dt}(t) = \lambda(X(t), t).$$

These characteristic curves are straight lines in the linear case ( $\lambda$  is constant) and general curves in the nonlinear case (see [Whi74] for more details).

Using Eq. (69), (72) becomes

$$\frac{\partial R}{\partial D} - \mu\lambda \frac{\partial R}{\partial B} = 0 \quad \forall \mathbf{Q} \in \mathbb{R}^2. \quad (73)$$

We have

$$\frac{\partial R}{\partial D} = \frac{\partial R}{\partial E} \frac{\partial E}{\partial D} = J^{-1} \frac{\partial R}{\partial E}.$$

But  $J^{-1} = \mu\lambda^2$  and, dividing (73) by  $\mu\lambda$ , we obtain

$$\lambda \frac{\partial R}{\partial E} - \frac{\partial R}{\partial B} = 0 \quad \forall \mathbf{Q} \in \mathbb{R}^2,$$

or more precisely

$$\boxed{\frac{\partial R}{\partial B} \pm \frac{1}{\sqrt{\mu\varepsilon_0(1 + \chi_1 + 3\chi_3 E^2)}} \frac{\partial R}{\partial E} = 0 \quad \forall \mathbf{Q} \in \mathbb{R}^2.} \quad (74)$$

We are now going to define Riemann invariants  $R$  in the case where the susceptibility is positive or zero, without loss of generality. Let us introduce

$$a = \varepsilon_0(1 + \chi_1), \quad b = 3\varepsilon_0\chi_3, \quad b \geq 0.$$

We define the scalar function  $u(\xi)$  by

$$u'(\xi) = \sqrt{\mu(a + b\xi^2)}. \quad (75)$$

We find

$$u(\xi) = \begin{cases} \xi\sqrt{a\mu} & \text{if } b = 0, \\ \xi u'(\xi) + a\sqrt{\frac{\mu}{b}} \log(\xi\sqrt{b\mu} + u'(\xi)) & \text{if } b > 0. \end{cases} \quad (76)$$

Note that  $u(\xi)$  is well defined since the constants  $a$ ,  $b$  and  $\mu$  are positive, and  $u'(\xi) > 0$ .

We can rewrite equations (74) as

$$\frac{\partial R}{\partial B} \pm \frac{1}{u'(E)} \frac{\partial R}{\partial E} = \frac{\partial R}{\partial B} \pm \frac{\partial R}{\partial u} = 0. \quad (77)$$

The general solutions of (77) are given by

$$R_k(u, B) = \Psi_k(u \mp B), \quad (78)$$

where  $\Psi_k$  is an arbitrary function of  $\mathbb{C}^1$ . If we choose  $\Psi_k(x) = x$  for  $k = 1, 2$  we obtain

$$R_1(u, B) = u + B, \quad R_2(u, B) = u - B, \quad (79)$$

where  $u(x)$  is given by (76).

**Proposition 2.** *The Riemann invariants  $R_k$  defined by (79) are constants on the characteristic curves i.e.*

$$\frac{dR_k}{dt}(X_k(t), t) = \left( \frac{\partial R_k}{\partial t} + \lambda_k \frac{\partial R_k}{\partial x} \right) (X_k(t), t) = 0. \quad k = 1, 2 \quad (80)$$

We verify below the validity of Eq. (80) for  $R_1$ , the demonstration being the same for  $R_2$  except for the sign.

**Proof 2.** We make use of (79) and we have for  $(\xi = t)$  or  $(\xi = x)$

$$\frac{\partial R_1}{\partial \xi} = \frac{\partial u}{\partial \xi} + \frac{\partial B}{\partial \xi} = \frac{\partial u}{\partial E} \frac{\partial E}{\partial \xi} + \frac{\partial B}{\partial \xi} = u'(E) \frac{\partial E}{\partial \xi} + \frac{\partial B}{\partial \xi}.$$

Eq. (80) becomes (for  $k = 1$ )

$$\frac{\partial R_1}{\partial t} + \lambda_1 \frac{\partial R_1}{\partial x} = u'(E) \frac{\partial E}{\partial t} + \frac{\partial B}{\partial t} + \lambda_1 \left( u'(E) \frac{\partial E}{\partial x} + \frac{\partial B}{\partial x} \right).$$

But, by definition (see (32) and (75)), we have

$$u'(E) = -\lambda_1^{-1} = \sqrt{\mu J}. \quad (81)$$

We thus deduce for  $(E, B)$  solution of (27) that

$$\frac{\partial B}{\partial t} + \lambda_1 u'(E) \frac{\partial E}{\partial x} = \frac{\partial B}{\partial t} - \frac{\partial E}{\partial x} = 0, \quad (82)$$

and

$$u'(E) \frac{\partial E}{\partial t} + \lambda_1 \frac{\partial B}{\partial x} = \sqrt{\mu J} \frac{\partial E}{\partial t} - \frac{1}{\sqrt{\mu J}} \frac{\partial B}{\partial x} = J \frac{\partial E}{\partial t} - \frac{1}{\mu} \frac{\partial B}{\partial x} = 0. \quad (83)$$

The function  $\Psi$  being arbitrary, we can construct an infinity of Riemann invariants for problem (27).

**Remark 4.** *In the linear case, we have  $u = E\sqrt{a\mu} = \frac{1}{c}E$  where  $c$  is the velocity of the waves in the underlying medium and the Riemann invariants are given by*

$$R_1(E, B) = \frac{1}{c}E + B, \quad R_2(E, B) = \frac{1}{c}E - B. \quad (84)$$

## B Rescaling of the equations

We rescale the physical quantities so that the electromagnetic fields and inductions share the same physical dimension and the speed light in vacuum  $c_0$  is dimensionless and is equal

Symbol	Name	Unit (S.I.)
<b>E</b>	Electric field	V/m (V: Volt)
<b>D</b>	Electric induction	C/m <sup>2</sup> (C: Coulomb)
<b>H</b>	Magnetic field	A/m (A: Ampère)
<b>B</b>	Magnetic induction	V s/m <sup>2</sup> (T: Tesla)
$\varepsilon$	Electric permittivity	C/V/m (F/m with F: Farhad)
$\mu$	Magnetic permeability	V s/A/m (H/m with H: Henry)

Table 2: Physical dimensions in the S.I. unit system.

to 1. We first recall the physical dimensions of the quantities appearing in the Maxwell system (1) as expressed in the S.I. unit system. We set

$$\begin{aligned}
\varepsilon_r(\mathbf{E}) &= \varepsilon(\mathbf{E})/\varepsilon_0, \quad \mu_r = \mu/\mu_0, \quad \tau = c_0 t, \\
\tilde{\mathbf{D}}(\tilde{\mathbf{E}}) &= \mathbf{D}(\mathbf{E})/\varepsilon_0 = \varepsilon_r(\mathbf{E})\mathbf{E} = \varepsilon_r(\tilde{\mathbf{E}})\tilde{\mathbf{E}} \quad (\tilde{\mathbf{E}} = \mathbf{E}), \\
\tilde{\mathbf{B}} &= c_0 \mathbf{B} = c_0 \mu \mathbf{H} = \mu_r (Z_0 \mathbf{H}) = \mu_r \tilde{\mathbf{H}},
\end{aligned} \tag{85}$$

where  $\varepsilon_0$ ,  $\mu_0$ ,  $Z_0 = \sqrt{\mu_0/\varepsilon_0}$  and  $c_0 = 1/\sqrt{\varepsilon_0\mu_0}$  respectively denote the electric permittivity, the magnetic permeability, the impedance and the speed of light in vacuum. With this change of variables, the Maxwell system (1) is unchanged

$$\frac{\partial \tilde{\mathbf{D}}}{\partial \tau} = \nabla \times \tilde{\mathbf{H}}, \tag{86a}$$

$$\frac{\partial \tilde{\mathbf{B}}}{\partial \tau} = -\nabla \times \tilde{\mathbf{E}}, \tag{86b}$$

In system (86),  $\tau$  is measured in meters and all the vector fields are given in V/m, while the definition of the electric permittivity (11) becomes a quantity without dimension

$$\varepsilon_r = \varepsilon_r(\tilde{\mathbf{E}}) = \left( \varepsilon_{L,r} + \chi_3 \|\tilde{\mathbf{E}}\|^2 \right), \tag{87}$$

where  $\varepsilon_{L,r} = 1 + \chi_1$  is the relative linear permittivity (without dimension) and the third order susceptibility  $\chi_3$  is still measured in (m/V)<sup>2</sup>.

## C An implicit analytical solution [PNTB09]

### C.1 Formulation of the analytical solution

We consider the 1d problem using the rescaled quantities (see section B)

$$\begin{cases} \frac{\partial E}{\partial t} - \mathcal{J}^{-1} \frac{\partial H}{\partial x} = 0, \\ \frac{\partial H}{\partial t} - \mu_r^{-1} \frac{\partial E}{\partial x} = 0, \\ \mathcal{J} = \varepsilon_{L,r} + 3\chi_3 E^2, \end{cases} \quad (88)$$

where  $E = E_z$ ,  $H = H_y$  and  $t$  ( $= \tau$  in section B) is measured in meters. The solutions  $(E, H)^\pm$  of problem (88) implicitly defined by

$$\begin{aligned} E^\pm(x, t) &= F(x \pm \lambda^\pm t), \\ H^\pm(x, t) &= \frac{1}{Z_r} G^\pm \left( \frac{3\chi_3 E^\pm(x, t)^2}{\epsilon_r} \right) E^\pm(x, t), \\ \lambda^\pm = \lambda(E^\pm) &= \frac{1}{\sqrt{\mu_r \mathcal{J}^\pm}}, \quad Z_r = \sqrt{\frac{\mu_r}{\epsilon_r}}, \quad \epsilon_r = 1 + \chi_1, \end{aligned} \quad (89)$$

where  $F$  is a  $C^1$  function verifying the condition

$$\exists M \in ]0, 1[ \text{ such that } \left| \frac{\partial F}{\partial E} \right| < M \quad (90)$$

and  $G^\pm$  is given by the series

$$\begin{aligned} G^\pm(\xi) &= \sum_{n=0}^{\infty} a_n^\pm \xi^n \\ a_n^+ &= (-1)^n \frac{(2n-3)!!}{2^n (2n+1)n!}, \quad n > 0 \\ a_0^+ &= -1 \\ a_n^- &= -a_n^+; \quad n \geq 0 \\ n!! &= \prod_{\substack{k=1 \\ k \text{ impair}}}^n k. \end{aligned} \quad (91)$$

The condition (90) is introduced to enforce the existence of the solution  $E$  when applying Banach's fixed-point theorem; the condition  $\chi_3 < 0$  is sometimes added<sup>1</sup>, however it is rarely verified in practice and is not necessary from our point of view.

We note that the functions with positive (respectively negative) exponent correspond to a wave traveling to the left (respectively right) on the  $x$ -axis.

If we want to solve problem (88) with the initial condition  $E(x, 0) = E_0(x)$  where  $E_0$  verifies

<sup>1</sup><http://www.optics.rochester.edu/workgroups/boyd/publications/fischer-g.html>

condition (90), we can look for the solution under the form (89) by setting  $F = E_0$ . However, this procedure is valid only for  $t \in [0, T_{\max}]$  for which  $F$  always verifies the (90), yielding the existence and unicity of the solution.

## C.2 Estimation of $T_{\max}$

Let  $F = E_0$  with  $E_0 \in C^1(\mathbb{R})$  and for  $(E = E^-)$  we have

$$\left| \frac{\partial F}{\partial E} \right| = 3t |\chi_3 E_0(x - \lambda t) E'_0(x - \lambda t) \lambda^{-3}|$$

From the condition (90) and for  $\chi_3 > 0$  we deduce an estimation of  $T_{\max}$

$$T_{\max} \approx \frac{\left( 3\chi_3 \|E_0\|_{\infty}^2 + \varepsilon_{L,r} \right)^{3/2}}{3|\chi_3| \|E_0\|_{\infty} \|E'_0\|_{\infty}}. \quad (92)$$

For  $\chi_3 = 0$  (i.e. in the linear case) we have that  $\frac{\partial F}{\partial E} = 0$  and the condition (90) is verified for any  $t > 0$ , and thus  $T_{\max} = +\infty$ .

## References

- [Bet09] K. Betzler. Nonlinear optics. [http://betzler.physik.uni-osnabrueck.de/Skripten/Nonlinear\\_Optics.php](http://betzler.physik.uni-osnabrueck.de/Skripten/Nonlinear_Optics.php), 2009. Lecture notes.
- [BKN11] K. Busch, M. König, and J. Niegemann. Discontinuous Galerkin methods in nanophotonics. *Laser and Photonics Reviews*, 5:1–37, 2011.
- [Bla13] E. Blank. *The Discontinuous Galerkin method for Maxwell’s equations. Application to bodies of revolution and Kerr-nonlinearities*. PhD thesis, Karlsruher Institut für Technologie, 2013.
- [CS01] B. Cockburn and C.-W. Shu. Runge-Kutta discontinuous Galerkin methods for convection-dominated problems. *J. Sci. Comp.*, 16(3):173–261, 2001.
- [de 00] A. de la Bourdonnaye. High-order scheme for a nonlinear Maxwell system modelling Kerr effect. *J. Comput. Phys.*, 160(2):500–521, 2000.
- [FLLP05] L. Fezoui, S. Lanteri, S. Lohrengel, and S. Piperno. Convergence and stability of a discontinuous Galerkin time-domain method for the 3D heterogeneous Maxwell equations on unstructured meshes. *ESAIM: Math. Model. Numer. Anal.*, 39(6):1149–1176, 2005.
- [FWR07] A.C. Fisher, D.A. White, and G.H. Rodrigue. An efficient vector finite element method for nonlinear electromagnetic modeling. *J. Comput. Phys.*, 225(2):1331–1346, 2007.
- [Got05] S. Gottlieb. On high order strong stability preserving Runge-Kutta and multi-step time discretizations. *J. Sci. Comp.*, 25(1–2):105–128, 2005.



- [HW02] J.S. Hesthaven and T. Warburton. Nodal high-order methods on unstructured grids. I. Time-domain solution of Maxwell's equations. *J. Comput. Phys.*, 181(1):186–221, 2002.
- [Jac99] J.D. Jackson. *Classical electrodynamics*. John Wiley & Sons, 1999.
- [JT97] R.M. Joseph and A. Taflove. FDTD Maxwell's equations models for nonlinear electrodynamics and optics. *IEEE Trans. Antennas and Propagation*, 45(3):364–374, 1997.
- [Lee79] B. Van Leer. Towards the ultimate conservative difference scheme. *J. Comput. Phys.*, 32:101–136, 1979.
- [LHvL83] P.D. Lax, A. Harten, and B. van Lee. On upstream differencing and Godunov type schemes for hyperbolic conservation laws. *SIAM Rev.*, 25(61):35–6, 1983.
- [O<sup>+</sup>10] A.F. Oskooi et al. Meep: A flexible free-software package for electromagnetic simulations by the fdtd method. *Comput. Phys. Commun.*, 181.3:687–702, 2010.
- [PNTB09] M. Pototschnig, J. Niegemann, L. Tkeshelashvili, and K. Busch. Time-domain simulations of the nonlinear Maxwell equations using operator-exponential methods. *IEEE Trans. Antennas and Propagation*, 57(2):475–483, 2009.
- [Shu13] C.-W. Shu. A brief survey on discontinuous Galerkin methods in computational fluid dynamics. *Adv. Math.*, 43:541–554, 2013.
- [Sjö07] D. Sjöberg. On uniqueness and continuity for the quasi-linear, bianisotropic maxwell equations, using an entropy condition. *PIER*, 71:317–339, 2007.
- [TH05] A. Taflove and S.C. Hagness. *Computational electrodynamics: the finite-difference time-domain method - 3rd ed.* Artech House Publishers, 2005.
- [Whi74] G.B. Whitham. *Linear and nonlinear waves*. Wiley, 1974.
- [ZJ93] R.W. Ziolkowski and J.B. Judkins. Full-wave vector Maxwell equation modeling of the self-focusing of ultrashort optical pulses in a nonlinear Kerr medium exhibiting a finite response time. *J. Opt. Sc. Am B*, 10(2):186–198, 1993.



**RESEARCH CENTRE  
SOPHIA ANTIPOLIS – MÉDITERRANÉE**

2004 route des Lucioles - BP 93  
06902 Sophia Antipolis Cedex

Publisher  
Inria  
Domaine de Voluceau - Rocquencourt  
BP 105 - 78153 Le Chesnay Cedex  
[inria.fr](http://inria.fr)

ISSN 0249-6399